A Compatibilized Composite of Recycled Polypropylene Filled with Cellulosic Fiber from Recycled Corrugated Paper Board: Mechanical Properties, Morphology, and Thermal Behavior

Zhidan Lin, Chao Chen, Zixian Guan, Shaozao Tan, Xiuju Zhang

College of Science and Engineering, Jinan University, Guangzhou 510632, People's Republic China

Received 31 October 2010; accepted 9 February 2011
DOI 10.1002/app.34321
Published online 29 June 2011 in Wiley Online Library (wileyonlinelibrary.com).

ABSTRACT: This article deals with the feasibility of using recycled corrugated paper board (rPF) as the reinforcing material for recycled plastics. The composites of recycled polypropylene (rPP) and rPF were prepared by extrusion compounding and injection molding, and the rPP/rPF composites compatibilized by maleic anhydride grafted PP (PP-*g*-MA), maleic anhydride grafted ethylene-1-octene copolymer (POE-*g*-MA), and maleic anhydride grafted styrene-ethylene-butylene-styrene copolymer (SEBS-*g*-MA) were also prepared. The crystallization and melting behavior, mechanical properties, thermal stability, and morphology of these composites were studied. The results indicated that rPF promoted the crystallization, enhanced the strength and toughness of rPP/rPF composites to some extent while decreased thermal stability at the same time. PP-*g*-MA and POE-*g*-MA improved the dispersion and interface adhesion of rPF, and further upgraded the mechanical properties and vicat softening temperatures. Among these compatibilizers, PP-*g*-MA was most favorable to the strength improvement while POE-*g*-MA was most favorable to the toughness improvement. As for SEBS-*g*-MA, it had no obvious modification effect. © 2011 Wiley Periodicals, Inc. J Appl Polym Sci 122: 2789–2797, 2011

Key words: poly(propylene)(PP); compatibilization; mechanical properties; morphology; thermal properties

INTRODUCTION

While paper products consume a large amount of forest resources, forests are declining at an alarming rate. To protect the environment, it is of great necessity to recycle the wasted paper. Among the recycled paper products, corrugated paper has taken a growing part. In China, the main material of corrugated paper is hardwood pulp, imported waste paper pulp and straw pulp. Generally, the recycled corrugated paper is only used for manufacturing corrugated paper board in turn. With the increase of recycling time, fibers in the waste paper pulp get shorter while the paper properties deteriorate. It is necessary to find new recycling methods of wasted corrugated paper. Recently, thermoplastics reinforced by cellulose fiber have been receiving considerable attention due to their low cost, low density, acceptable specific strength, good thermal insulation properties, reduced tool wear, reduced thermal and respiratory irritation, and renewable resources. Thermoplastics filled with cellulose fibers from recycled newspaper pulp after purification has been reported.[1–7] The worldwide production and consumption of plastics have resulted in a significant contribution to municipal solid waste. Among these plastic wastes, nondegradable polyolefin used as the packaging material has taken a great part. Its effective and safe disposal has been a pressing concern. In fact, corrugated paper boards are composites of cellulose fibers and polymer bonding agent, whose major constituents are polyvinyl alcohol, starch and polyacrylamide. Therefore, corrugated paper boards have the feasibility of being considered as cellulose fiber concentrates and applied into filled recycled polyolefin. However, no related report has been seen so far.

However, cellulose fibers are generally hydrophilic and are inherently incompatible with hydrophobic polyolefin such as polypropylene (PP). The key problem of using cellulose fibers to reinforce recycled polyolefin is the poor interfacial bonding between them. To overcome this difficulty, cellulose fibers were dealt with through physical methods,[8] chemical methods,[9,10] coupling agent modification,[11] and polymer compatibilizer modification[12–16] to obtain optimal interface bonding. Maleic anhydride grafted polypropylenes are often added as

Correspondence to: Z. Lin (linzd@jnu.edu.cn).
Contract grant sponsor: Fundamental Research Funds for the Central Universities of China; contract grant number: 21609711.
Contract grant sponsor: Technology of Guangdong Province, China; contract grant number: 2010A080804021.

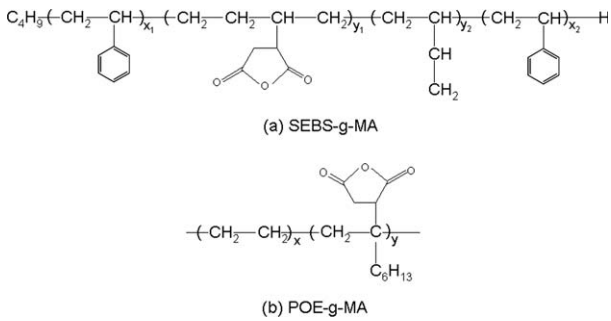

Figure 1 Chemical formula of POE-*g*-MA and SEBS-*g*-MA.

compatibilizers and gain favorable interface modification results.[14–16] Although higher interfacial adhesion improves the strength, the toughness of the composites would not be satisfactory. Impact modifiers such as ethylene block copolymer,[17] ethylene-methyl acrylate[18] and styrene/butadiene rubber[19] could modify the low toughness of PP reinforced by cellulose fibers.

The aim of this study is to avoid complicated recycling process of wasted paper products. PP/recycled corrugated paper board hybrid composites were prepared by directly crushing the recycled corrugated paper board into powder through mechanical disintegration, and then melt blending with recycled PP. The mechanical properties, morphology and thermal behavior of the composites were characterized, and the effect of compatibilizers on them was also investigated.

EXPERIMENTAL

Materials

The recycled polypropylene (rPP), with MI = 13.1 g/10 min at 200°C, was obtained by crushing the commercial recycled bottle marked with 100% PP from a salvage station in China. The recycled corrugated paper board was purchased from a salvage station in south China. PP-*g*-MA (with MI = 20 g/10 min at 200°C and 1.0 wt % of MA), POE-*g*-MA [with MI = 20 g/10 min at 200°C, 1.1 wt % of MA and the chemical formula in Fig. 1(a)] and SEBS-g-MA [with MI = 20 g/10 min at 200°C, 1.0 wt % of MA and the chemical formula in Fig. 1(b)] were supplied by China Guangzhou Lushan Chemical Materials.

Preparation of composites and test specimens

The recycled corrugated paper board was crushed into fluffy paper celluflours with the particle size less than 100 μm in a breaker with the rotation speed of 28,000 r min^{-1} and was abbreviated as rPF. The rPP, PP-*g*-MA, POE-*g*-MA, SEBS-*g*-MA, and rPF were dried at 80°C for 24 h and mixed according to the composition in Table I. The mixtures were blended in a twin-screw extruder at the temperature of 200°C. The extruded composites were cooled at room temperature and were crushed into small granules in a plastic breaker. All extruded composites were molded according to ASTM D638, ASTM D790, and ISO 179 using the injection molding machine at the temperature of 200°C to prepare tensile, flexural and Charpy impact test specimens.

Mechanical testing

Tensile, flexural, and impact tests were carried out according to ASTM Standard. For each test and each type of composite, five specimens were tested and the average values were reported. Tensile tests were conducted according to ASTM D 638 using a Universal Testing Machine (Zwick/Roell Z005, Zwick Roell Testing Machines) at a crosshead speed of 50 mm min^{-1}. Static flexural tests were carried out according to ASTM D 790 using the same Testing Machine mentioned above at a crosshead speed of 2 mm min^{-1}. Notched Charpy impact strength tests were conducted according to GB/T 1043 using a Universal Impact Testing Machine (ZBC-50, China Shenzhen SANS Testing Machine) and the notch was made by gear cutters.

TABLE I
Composition of rPP/rPF Composites and its Compatibilized Composites

Sample	rPP (wt %)	rPF (wt %)	PP-*g*-MA (wt %)	Sample	rPP (wt %)	rPF (wt %)	POE-*g*-MA (wt %)	SEBS-*g*-MA (wt %)
rPP	100	–	–	O5F10	85	10	5	–
F10	90	10	–	O5F20	75	20	5	–
F20	80	20	–	O5F30	65	30	5	–
F30	70	30	–	O5F40	55	40	5	–
F40	60	40	–	O2F30	68	30	2	–
P5F10	85	10	5	O8F30	62	30	8	–
P5F20	75	20	5	S5F10	85	10	–	5
P5F30	65	30	5	S5F20	75	20	–	5
P5F40	55	40	5	S5F30	65	30	–	5
P2F30	68	30	2	S5F40	55	40	–	5
P8F30	62	30	8					

Microstructure analysis

The impact specimens were frozen in liquid nitrogen for 3 h, and then quickly smashed. The fracture surfaces of the specimens were sputter-coated with gold before scanning electron microscope (SEM) analysis. The fracture surface morphology of the composites was observed on a Philips XL-30 ESEM microscope with an acceleration voltage of 15 kV.

Characterization of nonisothermal crystallization and melting behavior

A TA Instruments Q200 differential scanning calorimeter (DSC) was used to study the nonisothermal crystallization and melting behavior of rPP and all the rPP/rPF composites, and was calibrated using the melting temperature and enthalpy of a pure indium standard. About 8–9 mg of the sample was accurately weighted for DSC testing, and all measurements were performed in nitrogen atmosphere. A composite sample was rapidly heated to 220°C and held for 5 min to eliminate the heat history. Subsequently, it was cooled to 60°C at the cooling rate of 20°C min^{-1} for crystallization behavior study. And then, it was reheated to 220°C at 20°C min^{-1} for melting behavior study.

TGA analysis

The thermal decomposition behavior of the composites was studied by heating from 50 to 700°C at the heating rate of 20°C min^{-1} on a TA Instruments Q5000 thermogravimetry in nitrogen atmosphere.

Vicat softening temperature testing

The vicat softening temperature of the composites was tested on a heating deflection and vicat softening temperature measuring apparatus (GT2HV2000, Taiwan Gotech Testing Machines) according to ASTM D1525 Standard.

RESULTS AND DISCUSSION

Nonisothermal crystallization and melting behavior

Table II shows the nonisothermal crystallization and subsequent melting parameters of the rPP/rPF composites and its composites compatibilized by PP-*g*-MA, POE-*g*-MA, and SEBS-*g*-MA. It can be seen that the peak crystallization temperature (T_c^P) and onset crystallization temperature (T_c^{onset}) of PP in the rPP/rPF composites increased when rPF was added. The T_c^P rised from 111.66°C of pure PP to above 116°C of the rPP/rPF composites while T_c^P and T_c^{onset} changed slightly with the increasing content of rPF. This is in accordance with Luz's results.[20] As a kind of solid organic cellulose, the rPF did not melt during the compounding process. It acted as nucleating agent and changed the crystallization of the matrix around the rPF. This nucleating effect reached saturation when rPF content arrived at 10 wt %. Similarly, the T_m^P of rPP was improved when being blended with rPF. Moreover, the T_m^P of the composites increased with the increasing content of rPF, and changed slightly when rPF content was above 20 wt %. When the rPP/rPF composites were modified with 5 wt %

TABLE II
Nonisothermal Crystallization and Melting Parameters of rPP, rPP/rPF Composites, and rPP/rPF Composites Compatibilized by PP-*g*-MA, POE-*g*-MA, and SEBS-*g*-MA

Sample	T_c^P (°C)	T_c^{onset} (°C)	ΔH_c(J g^{-1})	T_m^P (°C)	ΔH_m (J g^{-1})
rPP	111.66	116.68	98.13	163.60	95.64
F10	117.09	122.68	103.38	165.64	97.03
F20	116.55	123.00	97.16	167.57	91.39
F30	116.11	122.47	89.77	168.20	83.97
F40	116.78	122.79	94.85	167.71	90.02
P5F10	118.94	123.47	100.81	163.30	96.31
P5F20	118.60	123.91	99.41	165.32	95.05
P5F30	117.55	124.08	94.60	166.98	90.16
P5F40	115.54	123.87	84.72	169.90	77.03
P2F30	117.36	124.84	79.62	168.40	77.73
P8F30	116.24	123.21	82.58	168.50	79.52
O5F10	114.46	121.81	92.00	168.52	86.17
O5F20	115.77	122.01	83.82	168.22	80.27
O5F30	116.69	122.23	92.37	166.81	89.27
O5F40	114.69	121.43	75.80	169.63	71.97
O2F30	116.15	122.30	88.53	167.88	86.22
O8F30	114.61	120.95	89.00	168.98	85.73
S5F10	112.82	118.24	93.30	165.97	88.96
S5F20	111.50	117.41	85.67	166.48	80.41
S5F30	109.01	116.62	81.55	169.24	77.65
S5F40	108.66	116.60	89.57	169.12	84.95

of PP-*g*-MA, the T_c^P and T_c^{onset} further increased compared with unmodified rPP/rPF composites, but the T_c^P decreased with the increasing content of rPF. Thus, with the help of PP-*g*-MA, the rPF dispersed well in PP matrix. Meanwhile, more nucleating sites were further brought about. When rPF content was fixedly 30 wt %, the T_c^P of rPP/rPF composite modified by 2 wt % of PP-*g*-MA was close to that of the composite modified with 5 wt % of PP-*g*-MA, while the T_c^P of the composite modified by 8 wt % of PP-*g*-MA decreased. This indicated that too much of PP-*g*-MA in the PP matrix might decrease the crystallization ability of PP. As rPF content was fixedly 30 wt %, the threshold of PP-*g*-MA appeared at about 5 wt %. When PP-*g*-MA content was fixedly 5 wt %, the T_m^P of PP in the rPP/rPF composites gradually increased with the increasing content of rPF. When rPF content was fixedly 30 wt %, the T_m^P also gradually increased with the increasing content of PP-*g*-MA. This might be due to the fact that the thermal conductivity of rPF is much smaller than PP, which delayed the release of melting heat of PP during nonisothermal DSC testing condition and led to the higher T_m^P. The more uniformly the rPF dispersed in PP, the more slowly the melting heat released. The crystallization and melting behavior of the rPP/rPF composites modified by POE-*g*-MA and SEBS-*g*-MA were different from that of the composites modified by PP-*g*-MA. The T_c^P and T_c^{onset} of the two formers were lower than that of the latter and unmodified rPP/rPF composites. When POE-*g*-MA content was fixedly 5 wt %, the T_c^P of PP in the composites gradually increased with the increasing content of rPF. Also, it decreased when rPF content reached 40 wt %. When rPF content was fixedly 30 wt %, the T_c^P of PP in the composites gradually decreased with the increasing content of POE-*g*-MA. According to the research result of our group that POE-*g*-MA had no nucleation effect on PP crystallization,[21] when its maleic anhydride group reacted with the surface of rPF, the crystallization of PP around rPF would be hindered and a lower T_c^P was observed. The T_m^P of rPP/rPF composites modified with POE-*g*-MA were obviously higher than that of pure PP, and it further proved that the poorer thermal conductivity of rPF led to the higher T_m^P. In the rPP/rPF composites modified with SEBS-*g*-MA, when SEBS-*g*-MA content was fixedly 5 wt %, the T_c^P decreased with the increasing content of rPF and were obviously lower than that of the unmodified composites and the composites modified with PP-*g*-MA or POE-*g*-MA. When rPF content was 20 wt %, the T_c^P of composites were even lower than that of pure PP. According to the research result of our group that SEBS-*g*-MA had no nucleation effect on PP crystallization,[21] the maleic anhydride group reacted with the surface of rPF and hinder the crystallization of PP around rPF. But the T_m^P is increased gradually also due to the poorer thermal conductivity of rPF. It was interesting that the heat of fusion ($\triangle H_m$) of the four kinds of PP/rPF composites decreased with the increasing content of rPF basically, but this rule changed at higher content of rPF. This might be due to the fact that the density of rPF is smaller than PP, the volume of rPF was larger than PP at the rPF content above about 30 wt % and the uniform dispersion of PP in rPF became much difficult at the melt blending condition. The larger phase of pure PP in PP/rPF composites with high rPF content led to the higher heat of fusion.

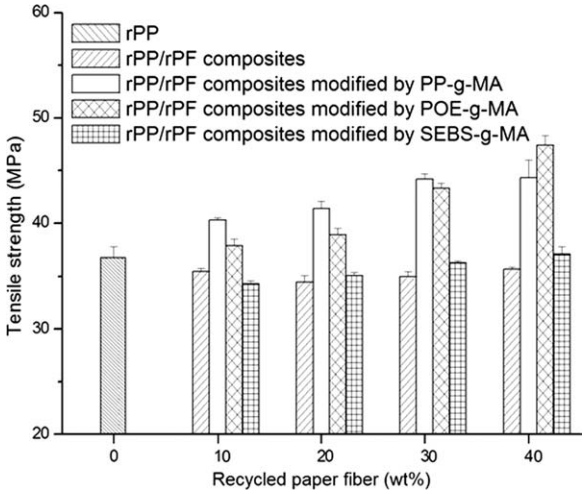

Figure 2 Tensile strength of rPP, rPP/rPF composites, and rPP/rPF composites compatibilized by PP-*g*-MA, POE-*g*-MA, and SEBS-*g*-MA.

Mechanical property

Figures 2–9 show the mechanical properties of rPP, rPP/rPF composites and rPP/rPF composites compatibilized by PP-*g*-MA, POE-*g*-MA, and SEBS-*g*-MA. It can be seen that the tensile strength (TS) of unmodified rPP/rPF composites somewhat declined, and elongation at break evidently dropped. With the increasing content of rPF, the flexural strength (FS), and flexural modulus (FM) of unmodified rPP/rPF composites gradually increased. The FS and FM of the F40 composite increased to 179 and 346% of that of rPP, respectively. These fully reveal that without modification, rPF still had strengthened and toughened effect to rPP. The TS and FS of rPP/rPF composites modified by PP-*g*-MA were all higher than that of rPP and corresponding unmodified rPP/rPF composites. The TS and FS of the P5F40 composite improved to 120 and 193% of that of rPP respectively, indicating that PP-*g*-MA could obviously modify the interface adhesion and improve the TS and FS at the same time. However, the increasing extent of FM was inferior to unmodified rPP/rPF composites. This may be due to the fact that the low

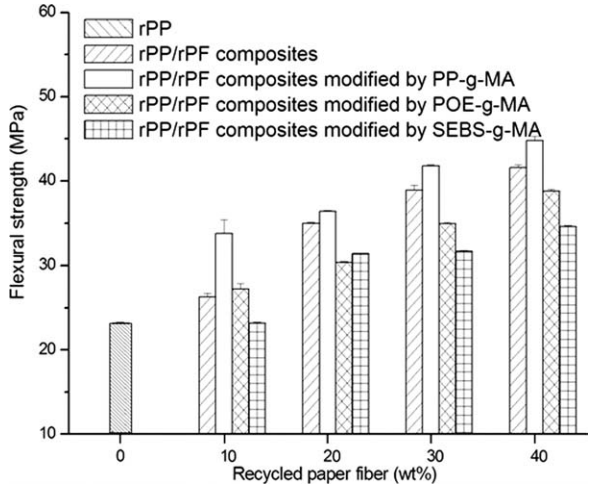

Figure 3 Flexual strength of rPP, rPP/rPF composites, and rPP/rPF composites compatibilized by PP-*g*-MA, POE-*g*-MA, and SEBS-*g*-MA.

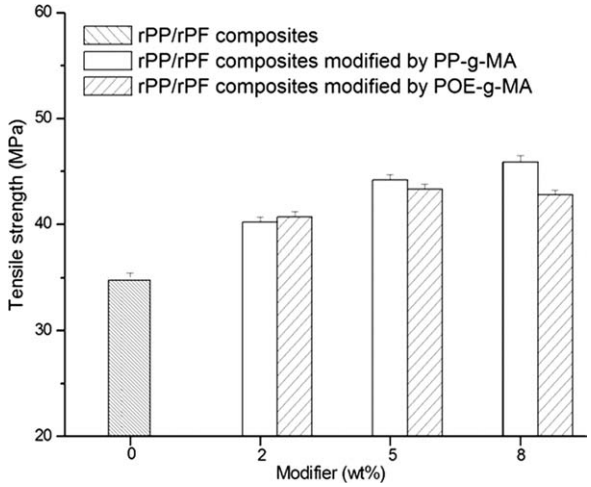

Figure 5 Tensile strength of rPP/rPF composite with 30 wt % of rPF and its composites compatibilized by different content of PP-*g*-MA and POE-*g*-MA.

FM of PP-*g*-MA affects the ability to resist the bending of rPP/rPF composites. The TS of rPP/rPF composites modified by POE-*g*-MA were higher than that of unmodified rPP/rPF composites while lower than that of rPP/rPF composites modified by PP-*g*-MA except O5F40 composite. The FS and FM of rPP/rPF composites modified by POE-*g*-MA were inferior to unmodified rPP/rPF composites and rPP/rPF composites modified by PP-*g*-MA. This may be due to the fact that the interface modification effect of POE-*g*-MA was lower than that of PP-*g*-MA and its FM was also inferior to that of PP-*g*-MA. The TS, FS and FM of rPP/rPF composites modified by SEBS-*g*-MA were all lower than unmodified rPP/rPF composites and rPP/rPF composites modified by PP-*g*-MA and POE-*g*-MA. The TS and FS were close to that of rPP. This may be due to the fact that SEBS-*g*-MA was incompatible with rPP and would not modify the interface adhesion. When the rPF content was fixedly 30 wt %, with the increasing content of PP-*g*-MA, the TS, FS, and FM of rPP/rPF composites modified by PP-*g*-MA presented upward trend. Meanwhile, with the increasing content of POE-*g*-MA, the TS of rPP/rPF composites modified by POE-*g*-MA slight increased, and the FS and FM gradually declined. These indicated that PP-*g*-MA would strengthen the interface adhesion of rPF and rPP, however, too much POE-*g*-MA would not benefit the interface modification.

The notched Charpy impact strength (IS) of unmodified rPP/rPF composites were higher than that of rPP, and the IS reached maximum of 2.11 kJ m^{-2} at 20 wt % of rPF. The IS of rPP/rPF composites modified by PP-*g*-MA further improved

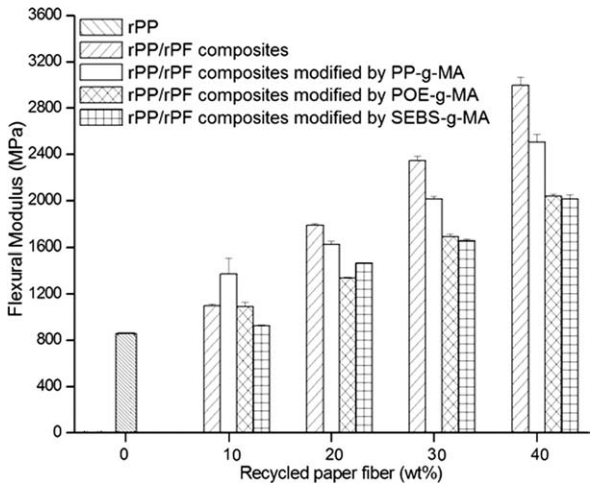

Figure 4 Flexual modulus of rPP, rPP/rPF composites, and rPP/rPF composites compatibilized by PP-*g*-MA, POE-*g*-MA, and SEBS-*g*-MA.

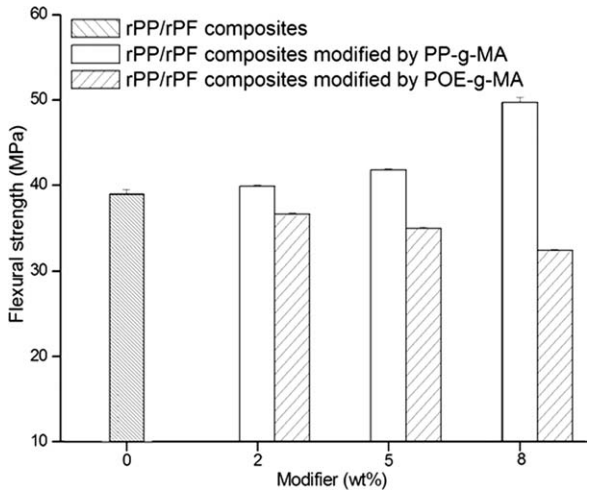

Figure 6 Flexual strength of rPP/rPF composite with 30 wt % of rPF and its composites compatibilized by different content of PP-*g*-MA and POE-*g*-MA.

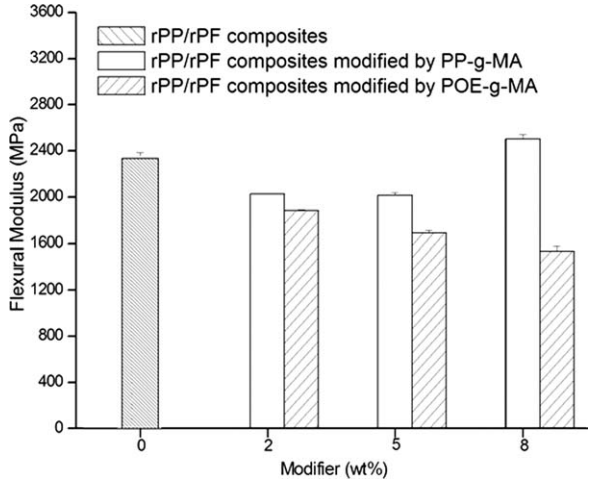

Figure 7 Flexual modulus of rPP/rPF composite with 30 wt % of rPF and its composites compatibilized by different content of PP-*g*-MA and POE-*g*-MA.

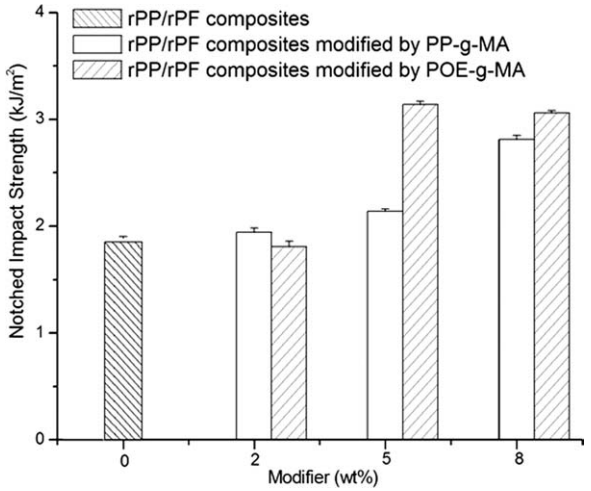

Figure 9 Notched Charpy impact strength of rPP/rPF composite with 30 wt % of rPF and its composites compatibilized by different content of PP-*g*-MA and POE-*g*-MA.

compared with unmodified rPP/rPF composites, and the IS reached maximum of 2.53 kJ m^{-2} also at 20 wt % of rPF. With the increasing content of rPF, the IS of rPP/rPF composites modified by POE-*g*-MA increased gradually and were higher than that of the two former. At 40 wt % of rPF, the IS reached maximum of 3.49 kJ m^{-2} which was 271% of that of rPP. However, the IS of rPP/rPF composites modified by SEBS-*g*-MA remained at about 2.5 kJ m^{-2} when rPF content was below 30 wt %, and slightly decline at 40 wt % of rPF. When the rPF content was fixedly 30 wt %, with the increasing content of PP-*g*-MA, the IS of rPP/rPF composites modified by PP-*g*-MA enhanced gradually. While the IS of rPP/rPF composites modified by POE-*g*-MA changed little at the rPF content above 5 wt %. These fully indicated that the compatibilizers had synergetic effect with rPF on the strengthening and toughening of the composites, and the POE-*g*-MA which was partly compatible with rPP showed best effect.

Thermal stability

Thermal decomposition (TG) behavior and heat distortion temperature revealed the material thermal stability at high temperature and service condition respectively. Figure 10 shows that TG and DTG curves of the rPP/rPF composites and its compatibilized composites with 30 wt % of rPF, and the related thermal stability parameters are provided on Table III. One decomposition stage occurred on the TG and DTG curves of rPP. However, two decomposition stages which differentiated at 376°C appeared on that of rPP/rPF composites and its compatibilized composites, and all the TG and DTG curves of

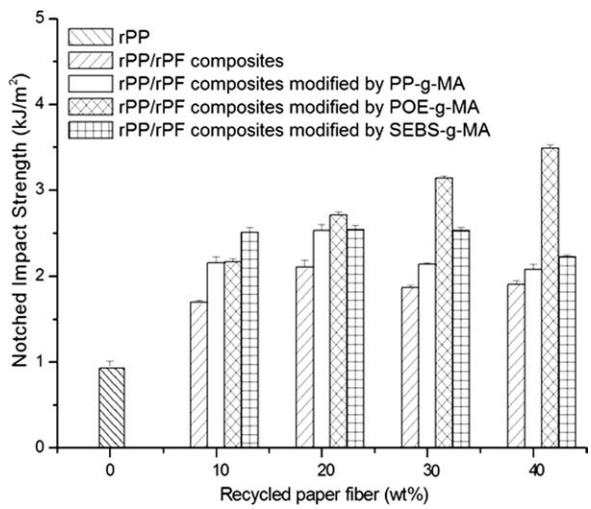

Figure 8 Notched Charpy impact strength of rPP, rPP/rPF composites and rPP/rPF composites compatibilized by PP-*g*-MA, POE-*g*-MA, and SEBS-*g*-MA.

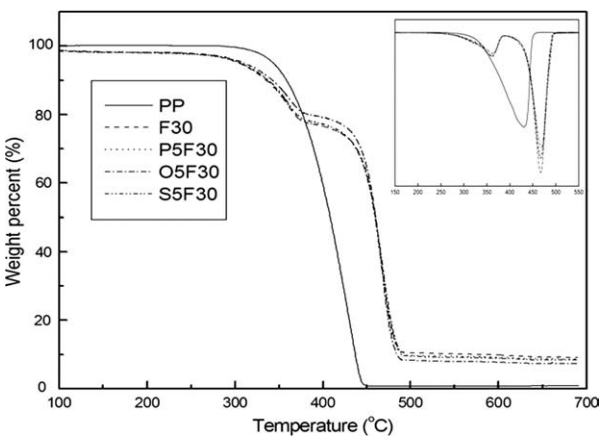

Figure 10 TG and DTG curves of rPP, rPP/rPF composite with 30 wt % of rPF and its composites compatibilized by PP-*g*-MA, POE-*g*-MA, and SEBS-*g*-MA.

TABLE III
Thermal Properties Data of rPP, rPP/rPF Composites, and rPP/rPF Composites Compatibilized by PP-*g*-MA, POE-*g*-MA, and SEBS-*g*-MA

Sample	Onset decomposition temperature (°C)	Decomposition peak temperature (°C)		Residual weight (wt %)	Vicat softening temperature (°C)
rPP	276.05	430.57		0.69	153.0
F30	267.96	360.14	466.85	12.14	157.0
P5F30	268.71	360.01	466.61	11.49	163.3
O5F30	268.02	362.27	467.56	10.31	157.4
S5F30	268.23	360.13	468.63	11.62	154.7

rPP/rPF composites were close. The three maleic anhydride-grafted compatibilizers slightly increased onset decomposition temperature of the rPP/rPF composites due to the fact that maleic anhydride and the —OH group on the surface of rPF exhibited strong bonding and delayed the decomposers release of rPF. The two decomposition stages were in turn corresponding to the decomposition of rPF and rPP. At the stage below 376°C, the decomposition of rPF advanced 8°C than that of rPP. This indicated that rPF decreased the thermal stability of rPP at high temperature condition, which is in accordance with Luz's results.[20] At the stage above 376°C, the decomposition of rPP in the composites delayed 50°C than that of pure rPP. These may be due to the fact that rPF decomposed and formed tar,[22] which dispersed in rPP uniformly and delayed the release of rPP decomposers. Thus, the second peak decomposition temperature increased from 430.57°C of rPP to above 466°C of the composites. The results of vicat softening temperature (VST) revealed that the VST of unmodified F30 composite was 4°C higher than that of rPP, while the addition of the compatibilizers with low VST further improved VST of the composites. These indicated that as a solid cellulose filler, rPF strengthened the ability of rPP to resist thermal deformation. The compatibilizers promoted the dispersion and the interface adhesion of rPF, and further improved this ability. Among the three compatibilizers, the rPP/rPF composite modified by PP-*g*-MA had the highest VST, indicating the strongest modification effect.

Morphology

Figure 11 shows the SEM micrographs of fracture surface of the rPP/rPF composites and its compatibilized composites with 30 wt % of rPF. It can be seen that the unmodified F30 composite [Fig. 11(a)] had a coarse surface with lots of exposed rPF rod-shaped particles. The clear interface between rPP and rPF and the smooth cavity attributed to the exfoliation of rPF were also observed. These indicated that rPF had a poor interface adhesion with rPP resin which can explain why the tensile strength of the unmodified rPP/rPF composites dropped. Compared with the F30 composite, the P5F30 composite [Fig. 11(b)] had a relatively smooth surface, and no rod-shaped particle and cavity was observed. Only a few rPF particles embedded in the rPP resin and the interface between them was tight. These indicated that PP-*g*-MA modified the interface adhesion between rPF and rPP very well, which leads to the improved tensile strength and flexural strength of the composites. On the fracture surface of O5F30 composite [Fig. 11(c)], the exposed rPF rod-shaped particles and the cavity attributed to the exfoliation of rPF were also observed, but their quantity was smaller than that of F30 composite. These indicated that POE-*g*-MA modified the dispersion and the interface adhesion between rPF and rPP to some extent, and in turn improved the tensile strength and flexural strength of the composites, but the modification effect was inferior to PP-*g*-MA. This may be due to the fact that POE-*g*-MA partly compatibilized with rPP. However, the condition similar to the F30 composite were seen on the fracture surface of S5F30 composite [Fig. 11(d)], indicating the worst modification effect of SEBS-*g*-MA among the three compatibilizers. This may be due to the fact that SEBS-g-MA was incompatible with rPP. Comparing the fracture surface condition of the composites with different content of compatibilizers, it can be seen that the dispersion and the interface adhesion of rPF turned better with the increasing content of PP-*g*-MA [see Fig. 11(b,e,f)], and the satisfying modification effect was achieved at 5 wt % of PP-*g*-MA. A similar rule was observed on the composites compatibilized by POE-*g*-MA [see Fig. 11(c,g,h)], but the satisfying modification effect was achieved at 8 wt % of POE-*g*-MA.

CONCLUSIONS

The rPF exhibited heterogeneous nucleation and promotion effect on the rPP crystallization. The PP-*g*-MA and POE-*g*-MA facilitate the dispersion of rPF and strengthened its promotion crystallization effect to PP, while the SEBS-*g*-MA retarded this effect. The addition of rPF improved the strength and toughness of rPP, but the interface adhesion between them was still poor. The addition of PP-*g*-MA and POE-*g*-MA modified the dispersion of rPF and the

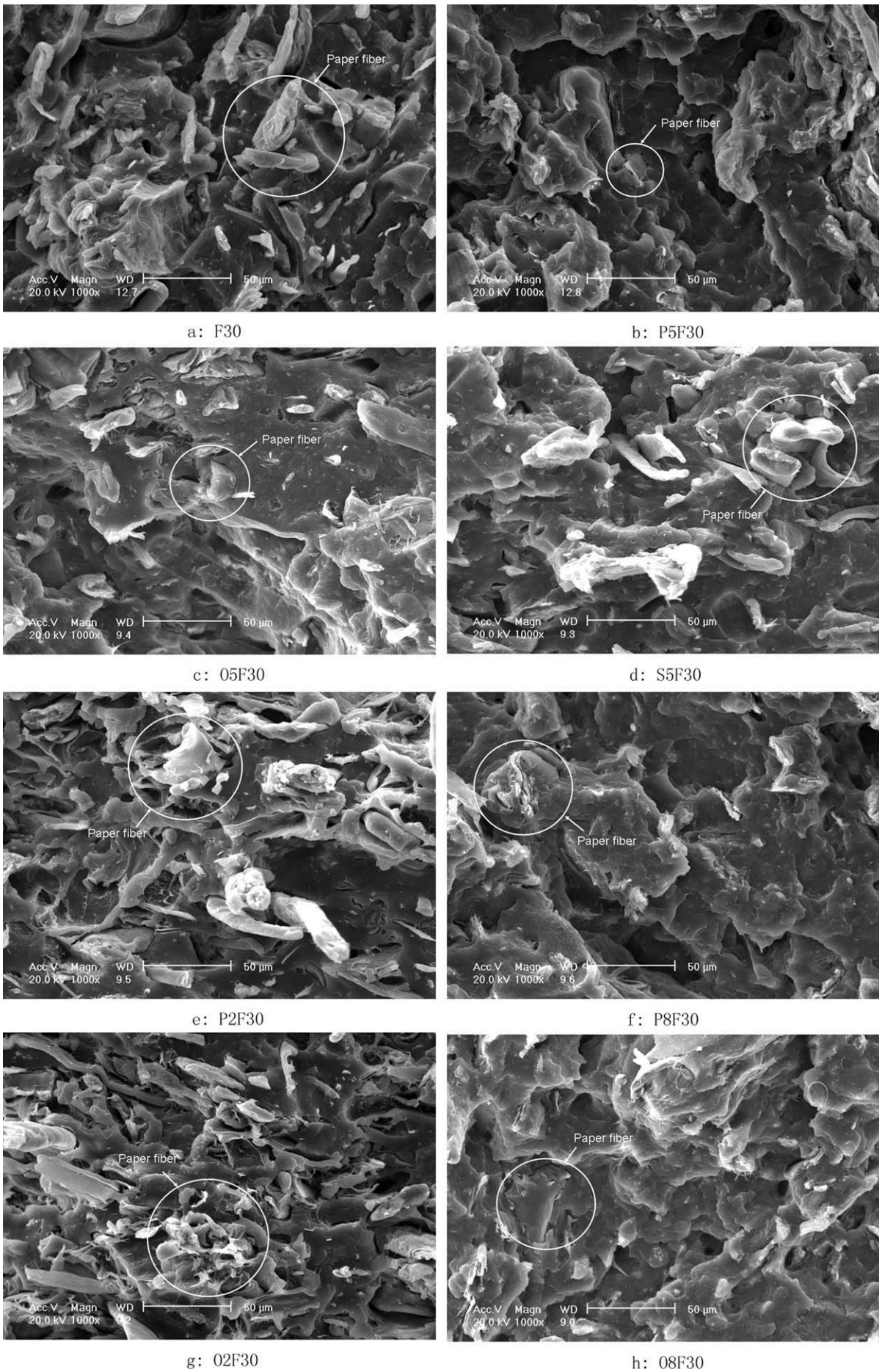

Figure 11 SEM micrographs of rPP, rPP/rPF composites, and rPP/rPF composites compatibilized by PP-*g*-MA, POE-*g*-MA, and SEBS-*g*-MA.

interface adhesion between rPP and rPF, and further upgraded the strength and toughness of the composites. Moreover, the compatibilizers resulted in a strong surface bonding by the reaction between maleic anhydride and the —OH group on the surface of rPF and the molecule entanglement with rPP, which made for the improvement in vicat softening temperature of the composites. Among these compatibilizers, PP-*g*-MA was most favorable to the strength improvement of rPP/rPF composites; POE-*g*-MA benefited the toughness improvement most while SEBS-*g*-MA had no obvious modification effect. To sum up, rPF can be a good substitution for the mineral reinforced material such as glass fibers to strengthen the recycled plastics.

References

1. Ashori, A.; Nourbakhsh, A. Waste Manage 2009, 29, 1291.
2. Huda, M. S.; Drzal, L. T.; Mohanty, A. K.; Misra, M. Compos Sci Technol 2006, 66, 1813.
3. Qiao, X. Y.; Zhang, Y.; Zhang, Y. X. J Appl Polym Sci 2004, 91, 2320.
4. Qiao, X. Y.; Zhang, Y.; Zhang, Y. X.; Zhu, Y. J Appl Polym Sci 2003, 89, 513.
5. Kanie, O.; Tanaka, H.; Mayumi, A.; Kitaoka, T.; Wariishi, H. J Appl Polym Sci 2005, 96, 861.
6. Baroulaki, I.; Karakasi, O.; Pappa, G.; Tarantili, P. A.; Economides, D.; Magoulas, K. Compos Part A Appl S 2006, 37, 1613.
7. Huda, M. S.; Drzal, L. T.; Mohanty, A. K.; Misra, M. Compos Part B Eng 2007, 38, 367.
8. Ragoubi, M.; Bienaime, D.; Molina, S.; George, B.; Merlin, A. Ind Crop Prod 2010, 31, 344.
9. Danyadi, L.; Moczo, J.; Pukanszky, B. Compos Part A Appl S 2010, 41, 199.
10. Borysiak, S. Polym Bull 2010, 64, 275.
11. Hong, H. Q.; Xu, H. X.; He, H.; Liu, T.; Jia, D. M. Plast Rubber Compos 2009, 38, 21.
12. Hong, C. K.; Kim, N.; Kang, S. L.; Nah, C.; Lee, Y. S.; Cho, B. H.; Ahn, J. H. Plast Rubber Compos 2008, 37, 325.
13. Fuqua, M. A.; Ulven, C. A. J Biobased Mater Biol 2008, 2, 258.
14. Yuan, Q.; Wu, D. Y.; Gotama, J.; Bateman, S. J Thermoplast Compos Mater 2008, 21, 195.
15. Bouza, R.; Lasagabaster, A.; Abad, M. J.; Barral, L. J Appl Polym Sci 2008, 109, 1197.
16. Nakatani, H.; Hashimoto, K.; Miyazaki, K.; Terano, M. J Appl Polym Sci 2009, 113 2022.
17. Khan, M. A.; Ganster, J.; Fink, H. P. Compos Part A Appl S 2009, 40, 846.
18. Sombatsompop, N.; Yotinwattanakumtorn, C.; Thongpin, C. J Appl Polym Sci 2005, 97, 475.
19. Hristov, V. N.; Vasileva, S.; Krumova, M.; Lach, R.; Michler, G. H. Polym Compos 2004, 25, 521.
20. Luz, S. M.; Del Tio, J.; Rocha, G. J. M.; Goncalves, A. R.; Del Arco, A. P., Jr. Compos Part A 2008, 39, 1362.
21. Shen, H.; Wang, Y.; Mai, K. Thermochim Acta 2007, 457, 27.
22. Brown, M. E. Introduction to Thermal Analysis Techniques and Applications; Chapman and Hall: London, 1988.